## Supplemental Materials

## Methods

### *Surgical preparation for electrophysiology and imaging*

Mice were anesthetized using urethane (1.5 g/kg i.p. Sigma-Aldrich U2500; (1)) supplemented with isoflurane (~0.5%), if necessary. Body temperature was monitored and maintained at 36 - 37°C using a water bath blanket. Once anesthetized, the head was stabilized in a stereotaxic frame with ear bars and an omega-shaped head bar was mounted on the skull with glue and dental cement. A 2 mm craniotomy was then performed, centered over the hindpaw region of primary somatosensory cortex, at 1.5 mm from the midline and 1.0 mm from the bregma, and the dura was left intact. This cranial window was immediately adjacent to the injury window. The craniotomy was filled with 2% agarose (mixed in artificial cerebrospinal fluid; in mM: 124 NaCl, 1.3 $CaCl_2$, 3 KCl, 2 $MgSO_4$, 1.4 $NaH_2PO_4$, 26 $NaHCO_3$ and 11 glucose) in order to keep the cortical surface moist and dampen the movement associated with animal breathing. The head bar was screwed onto a metal post, which was attached to the stage. The cranial window was then submerged with ACSF for the entire experiment. Neuronal recordings were made ~2.0 mm from the center of the CCI lesion (**Figure 1A**).

### *Intrinsic signal imaging of spreading depolarization*

Male C57BL/6J mice were used to avoid known sex-linked effects on spreading depolarization (SD) susceptibility (2). Animals were anesthetized via isoflurane (5% induction, 1.5%-0.8% maintenance) and mounted to a stereotaxic frame. Monitoring was as above, supplemented with monitoring of respiratory rate as an additional proxy for anesthetic depth (RR: 84-96 bpm). The right parietal bone was exposed, thinned to transparency 1 mm from

sagittal suture, bregma, lambda, and temporal ridge, and coated with silicone oil in preparation for imaging (3). SD induction burr hole was placed 0.5 mm lateral to the window. The cortex was illuminated via a white light-emitting diode and OIS (optical intrinsic signal) was collected with high-sensitivity monochrome CCD Camera (Mightex USB 2.0). Imaging parameters were adjusted via BUFCCD Camera App [resolution: 696x520 pixels (1:2 bin), CCD freq. 28 MHz, and frame time (0.1 ms) 10, exposure time 20 ms]. Images were acquired at 0.5 Hz for 2 hours, controlled by a Master-8 pulse generator (AMPI). A 15-minute baseline was established to ensure SDs that were not induced by the surgical preparation. Data was excluded from analysis if SD was present in baseline recordings. A 1 M KCl (potassium chloride) solution was delivered via syringe pump (WPI SP100i) through a 30Gx1in (regular bevel; BD PrecisionGlide™ Needle) syringe needle, placed at the corner of the burrhole, not touching cortex, at 1 ml/h for duration of recording. Excess KCl was wicked from a small depression drilled on the lateral side of burr hole using lens tissue. Offline analysis of SD transients was made with ImageJ (3, 4).

***Histology***

*Tissue Processing:* 48 h after CCI or sham surgery, mice were anesthetized with isoflurane and then perfused transcardially with cold phosphate buffered saline (PBS) followed by a fixative containing 4% paraformaldehyde (PFA) in PBS. After the brain was removed, it was postfixed in PFA for 24 hours and then stored in PBS until it was sectioned. Coronal sections 30 μm in thickness were cut using a tissue slicer (Leica Biosystems) and mounted on Superfrost/Plus slides. Sections were collected from bregma +2.0 to −3.0 mm that included the cortical impact site.

*Flurojade-B (FJB) Staining:* Staining was performed per published methods (5). Briefly, sections were incubated in following solutions: 100% alcohol, 3 min; 70% alcohol, 1 min; distilled water, 1 min; 0.04% potassium permanganate, 15 min; $dH_2O$, 1 min; 0.001% FJB in acetic acid, 30 min; $dH_20$, 3 times, 1 min. Stained sections were dried at room temperature overnight, were immersed in xylenes and then cover slips were applied using DPX mounting media. FJB-stained slices were imaged using a Hamamatsu Nanozoomer 2.0 HT (Olympus) at 20X magnification.

**Western blot**

Western blot was performed similar to our published methods (6). Briefly, mice were anesthetized and sacrificed with overdose of isoflurane, the brain was rapidly removed, and the somatosensory cortex was dissected and placed in ice-cold buffer (0.1 M PBS). Frozen tissues were homogenized in ice-cold homogenization buffer (10 mM $NaPO_4$, 100 mM NaCl, 10 mM Na pyrophosphate, 25 mM NaF, 5 mM EDTA, 5 mM EGTA, 2% Triton X-100, 0.5% Deoxycholate, 1 mM Na vanadate, pH 7.4) with a homogenizer, in the presence of protease inhibitors (complete mini, Roche, in fresh 100 mM Phenylmethylsulfonyl fluoride (PMSF) dissolved in ethanol). Tissue samples were briefly sonicated and lysed using the buffer, and centrifuged at 14,000 rpm for 5 min at 4°C. The supernatant was collected and protein was measured using the DC Protein Assay (Bio-Rad, Hercules, CA). Expression of Glyceraldehyde 3-phosphate dehydrogenase (GAPDH) was used as a loading control. Samples from sham and CCI mice were run in parallel. Optical density measurements were performed using ImageJ software and normalized to total protein levels (25 µg total protein). Protein samples (25 µg) were fractionated by SDS-PAGE (sodium dodecyl sulfate–polyacrylamide gel electrophoresis)

and transferred to a polyvinylidene difluoride (PDVF) membrane. After incubation with 10% nonfat milk in 1xPBS for 60 min, the membrane was further incubated with polyclonal antibodies against KCC2 (1:1,000, Millipore; product no. 07-432) or NKCC1 (1:500, Millipore; product no. AB3560P), or a monoclonal β-tubulin antibody (1:10,000, Sigma Aldrich; product no. T5201) at RT for 2 h. The blots were then incubated with a 1:2000 dilution of horseradish peroxidase-conjugated anti-rabbit IgG (GE Healthcare; product no. NA934) or anti-mouse antibodies (1:2000, GE Healthcare; product no. NA931) for 2 h at RT. Blots were visualized with enhanced chemiluminescence (Amersham/GE Healthcare). Optical density measurements were performed using NIH Image J software and quantified as optical density per 25 µg of total protein.

## Results and Discussion

### *Cell size measurements during calcium activity*

Because we used an activity-dependent cytosolic calcium sensor, whose response characteristics might affect our area measurements, we only measured neuronal cross-sectional area from recordings of baseline calcium activity, during which ~96% of neurons were inactive (the small percentage of active neurons was not included in primary analysis). A low number of active cells during baseline is not unexpected, as layer 2/3 pyramidal neurons tend to fire fewer action potentials in vivo under anesthesia (7). We also analyzed the small percentage of active neurons from Thy1-GCaMP6s mice to determine whether the baseline [$Ca^{+2}$] changes had an effect on area measurements. We found no changes (3/6 neurons), increases (2/6 neurons), or decreases (1/6 neurons) in cross-sectional area during calcium activity compared to baseline (with no activity). We concluded that changes in GCaMP fluorescence during neuronal activity may

modestly affect changes in cross-sectional area measurements, though with the small number and inconsistent direction of change it is difficult to be certain. In any case we conservatively elected to omit analysis of active neurons in order to prevent any possible biasing of results.

***Mechanisms of reduced excitatory input onto pyramidal neurons after TBI***

We observed a dramatic reduction in the frequency of excitatory currents after CCI (**Figure 2J,K**). We hypothesize that these are a consequence of the decreased intrinsic membrane excitability mediated by neuronal swelling. Alternatively, they might reflect a decreased number of excitatory synapses, decreased rate of action potential (AP) discharge from excitatory presynaptic neurons, decreased probability of release from terminals, or decreased size of the readily releasable pool (9, 10) after injury. We did observe a substantial loss of cortical neurons close to the lesion site in animals exposed to CCI (**Figure 1A,B**); thus, it is possible that a loss of axonal processes due to neuronal death could result in a reduction in the number of synaptic inputs in the 'penumbral' region (just outside area of neuronal death) we recorded. We also observed a reduction in AP rate (**Figure 3D)**, which could have contributed to the reduction in excitatory currents and might be due to neuronal loss rather than intrinsic excitability changes. Finally, other mechanisms, e.g. plasticity- or injury-based reduction in synaptic input (11), are possible and cannot be ruled out. However, unlike these alternative mechanisms, the intrinsic membrane changes provide a unifying explanation for all the behavior we observed.

***Possible role for potassium and Ih currents in excitability changes after TBI***

Intrinsic mechanisms besides neuronal swelling could contribute to changes in network activity. We observed decreases in up state area under the curve (AUC) in CCI neurons which are

mainly attributable to decreases in duration. We also observed reduced frequency of AP firing in layer 2/3 pyramidal neurons (**Figure 3D**). A reduction in AP firing could recruit activity-dependent potassium channels less efficiently, leading to longer up states (12). However, we observed shorter up states in CCI neurons associated with reduced neuronal firing. Up state duration can also be modulated by hyperpolarization-activated cyclic nucleotide–gated (HCN) channel mediated Ih currents (13), possibly by decreasing the input resistance ($R_{in}$), which can effectively shunt synaptic input (14, 15). Ih currents are enhanced in CA1 pyramidal neurons at 24 h post-CCI injury (16). However, to our knowledge there is no evidence of *cortical* Ih currents affected by TBI. Moreover, it is also known that only negligible Ih currents can be recorded from layer 2/3 pyramidal neurons (17, 18) [Suryavanshi, Brennan, unpublished observations]. Changes in Ih currents also affect neuronal membrane potential (19), and we found no changes in membrane potential (**Figure 2B**).

***Reduction in presynaptic release probability in neurons of CCI mice***

Sensory-evoked excitatory post-synaptic potentials (EPSPs) displayed two types of behaviors when stimuli were paired at an interstimulus interval of 200 ms. In most cases (82%, 9 of 11 neurons from both sham and CCI mice), sensory stimulation paired at time intervals of 200 ms produced a 20-30% depression in EPSP. In other cases (18%, 2 of 11 neurons), the paired-pulse protocol induced a facilitation in EPSP amplitude. On averaged data, a depression was observed in the $2^{nd}$ response in neurons of both sham and CCI mice. This depression was larger in neurons of CCI mice relative to sham animals ($p = 0.02$, Mann-Whitney test; n = 4 neurons, 4 mice per group; **Supplemental Figure 1**). This suggests decreased transmitter release probability after injury.

### *Spontaneous spreading depolarization after CCI*

Spreading depolarization (SD) is known to occur in response to CCI (20, 21). We recorded spontaneously occurring SDs (without KCl stimulus) for 4 h beginning immediately after CCI, in vehicle and bumetanide-treated animals. We consistently observed a single episode of SD immediately after CCI injury, but did not observe subsequent SDs in the 4 h recording period (except in one CCI-bumetanide animal with one full and 3 partial SDs after CCI). We did not observe differences in SD frequency between groups, though there was a significant difference in duration of SD, with CCI-bumetanide animals showing the shortest duration of SD ($p = 0.01$, two-sided Mann-Whitney test; n = 4-5 mice per group; **Supplemental Figure 3**). No significant differences in SD speed were observed between treatments ($p > 0.05$, two-sided Mann-Whitney test; n = 5-6 mice per group).

### *Role of SD-associated neuronal edema in the response to TBI*

SD is known to occur after TBI (20, 21) (our data). SD is also known to induce edema in both neuronal somata and dendrites (22, 23), ([Sawant-Pokam, Brennan,], unpublished observations). The mechanisms of this edema, which is specific to neurons (astrocytes are not observed to swell (22)) are incompletely understood at this time. There is also recent work showing that SD involved in stroke contributes to post-stroke edema, through SD-induced vasoconstriction and aquaporin-4-mediated perivascular glymphatic flow (24). The question arises of whether the neuronal edema we observed is due to TBI-associated SD, and whether the effects of bumetanide might be due to suppression of post-TBI SD. We found that bumetanide treatment had no effect on either the frequency or speed of SD initiated after CCI injury. The duration of SD was reduced

with bumetanide treatment, but the implications of this are unclear (**Supplemental Figure 3**). Importantly we observed (with one exception) only one SD event in all animals in the four-hour recording period after CCI – this agrees with prior work (25). There are two implications: firstly, the single SD induced by CCI is likely extraordinarily difficult to suppress, as it involves, the rapid destruction of large volumes of tissue, with the consequent release of 145 mM $[K^+]_e$ from lysed cells (26). Second, due to the presence of one difficult to suppress SD event, there is very little signal to noise for the comparison of vehicle and bumetanide treatment. Thus our results should not be taken as an indication of inefficacy of bumetanide suppression of SD under other circumstances.

Importantly however, the bumetanide treatment we used to test for SD suppression was effective in reducing neuronal edema (**Figure 4A**). The fact that this bumetanide dose did not affect SD incidence suggests that its effect on neuronal volume is independent of SD.

***Possible effects of bumetanide on astrocytic cation chloride cotransporters***

Astrocytic swelling has been reported to have effects on network excitability, possibly through increases in extracellular glutamate (27–29) and activation of NMDAR-mediated slow inward currents in neurons (30). As bumetanide is known to reduce astrocytic swelling observed after TBI (31), it is possible that we saw network effects resulting from astrocytic as well as neuronal manipulation. However, one would predict that reducing astrocyte swelling with bumetanide would *decrease* synaptic and network excitability. Instead, bumetanide had the opposite effect, increasing the frequency of excitatory currents, area-under-curve of up states and amplitude of sensory-evoked potentials. Though our data do not rule out the possibility of

bumetanide effects on astrocytes, we conclude that the increased network excitation we observed after bumetanide treatment is mediated by its effects on neurons.

***Reducing neuronal edema increases network excitability when bumetanide administered immediately post-CCI***

To improve potential translation of the protective effects of bumetanide on neuronal edema to clinical settings, we injected bumetanide post-CCI. Using both synapsin1-driven-GCaMP6f-injected and Thy1-GCaMP6s mice (cell sizes were comparable between two methods; see **Supplemental Figure 8**), the cross-sectional area of neuronal soma was significantly larger in CCI mice versus sham mice, consistent with results observed between sham and CCI groups. Moreover, neurons of CCI-bumetanide mice had smaller somatic area versus CCI-vehicle treated neurons ($p = 0.0008$, one-way ANOVA with Bonferroni's multiple comparisons; CCI-bumetanide vs vehicle: $***p < 0.001$, CCI-vehicle vs sham-vehicle: $**p < 0.01$; n = 33-75 neurons, 4 mice per group; **Supplemental Figure 4A**).

Next we assessed whether the reduction of neuronal edema with post-CCI bumetanide treatment would produce an effect on excitability, similar to what we observed with bumetanide pre-CCI treatment. Using the minimal clonic seizure test in animals injected with bumetanide post-CCI, we saw increases in the percentage of animals exhibiting seizures in CCI-bumetanide treated animals, compared to CCI-vehicle (CCI-bumetanide: 50 %, CCI-vehicle: 17 %, sham-vehicle: 22 %, sham-bumetanide: 38 %; ChiSqu test; CCI- bumetanide vs vehicle: $p = 0.04$; n = 8-12 mice per group; **Supplemental Figure 4B**). Thus, consistent with our bumetanide pre-CCI treatment, we

observed an increased susceptibility to seizures when we reduced edema with bumetanide post-CCI treatment (**Figure 7**).

***Effect of bumetanide administered 48 h post CCI***

Administration of bumetanide prior and post- to CCI produced a marked reduction in neuronal swelling 48 h later (**Figure 4A**, **Supplemental Figure 4A**). We tested whether this protective effect on edema could still be obtained if treatment was initiated 48 h after injury. In contrast to pre-CCI/sham bumetanide treatment, 48 h post-CCI administration in Thy1-GCaMP6s mice had no effect on neuronal surface area ($p = 0.001$, Bonferroni's multiple comparisons test; CCI-vehicle vs sham-vehicle: $^{**}p < 0.01$ and CCI-bumetanide vs sham- bumetanide: $^{*}p < 0.05$; n = 42-55 neurons, 4 mice per group; **Supplemental Figure 5A**).

We next analyzed network excitability assessed as seizure susceptibility in sham and CCI mice subjected to vehicle and bumetanide treatments at 48 h post-CCI/sham. As expected based on neuronal edema results, we did not see any change in the percentage of animals exhibiting seizures between CCI-bumetanide and CCI-vehicle treated animals at the 5 mA stimulus intensity (CCI-bumetanide: 30 %, CCI-vehicle: 40 %, sham-vehicle: 10 %, sham-bumetanide: 20 %; $p > 0.05$, ChiSqu test; n = 10 mice per group; **Supplemental Figure 5B**). Thus, the effects on neuronal size and excitability observed with pre- and post-treatment of bumetanide is reduced when the treatment is delayed for 48 h post-injury. This indicates that there are differences in the mechanism of this edema between 2 and 48 h post injury (see **Discussion**).

***Bumetanide effects on network excitability 48 h after CCI are likely due to changes in cotransporter gene expression***

Bumetanide has a half-life of 47 minutes in mice (32); thus it is highly unlikely that the effects we observed 48 h after treatment could be due to binding of NKCC1 (or KCC2) by the drug. We tested the effects of bumetanide delivered 30 min before CCI on the expression of NKCC1 and KCC2, 2 h after CCI. Both KCC2 and NKCC1 expression were increased in bumetanide- compared to vehicle-treated CCI cortex (KCC2 - $p = 0.005$, Kruskal-Wallis test with Dunn's multiple comparisons; CCI- bumetanide vs vehicle: $^{**}p < 0.01$; CCI-bumetanide vs sham-bumetanide: $p > 0.05$, CCI-vehicle vs sham-vehicle: $^{*}p < 0.05$; n = 5-7 mice per group; NKCC1 - $p = 0.008$, Kruskal-Wallis test with Dunn's multiple comparisons; CCI-bumetanide vs vehicle: $p < 0.05$; CCI-bumetanide vs sham-bumetanide: $p < 0.01$, CCI-vehicle vs sham-vehicle: $p > 0.05$; n = 5-7 mice per group; **Supplemental Figure 6A,B**). This resulted in an effective reversal of the increased NKCC1/KCC2 ratio observed after CCI with vehicle treatment (**Supplemental Figure 7**).

We also tested whether bumetanide pretreatment (prior to CCI) was required for its effects. We delivered bumetanide immediately after CCI and recorded neuronal volume and seizure susceptibility 48 h after CCI. The phenotype was similar to bumetanide delivered prior to injury, with a normalization of neuronal volume and an increase in seizure susceptibility (**Supplemental Figure 4**, compare with **Figure 4A, 7**).

Finally, we tested for effects of bumetanide when the drug was delivered at the 48 h time point, 45 min prior to measurement of neuronal volume and seizure susceptibility. In contrast to

bumetanide delivered either 30 min before or immediately after CCI, there was no difference in neuronal volume compared to vehicle treated animals (i.e. edema was not reduced) and there was no difference in seizure susceptibility (i.e. it was similar to vehicle treatment) (**Supplemental Figure 5**, compare with **Figure 4A, 7, Supplemental Figure 4**). Taken together these data suggest that the effects of bumetanide are due to changes in cotransporter expression, rather than direct cotransporter binding by the drug.

***Mechanisms of SD and seizure susceptibility after TBI***

Like neuronal excitability, SD and seizure susceptibility are subject to parameters that may exert opposite influences. In part, these parameters are identical: increased neuronal volume should, other things equal, be associated with a decrease in excitability, increased neuronal chloride content with an increase. However, for network events like SD and seizures, the characteristics of the extracellular space become potentially important. Neuronal (or astrocytic) swelling restricts the interstitial space, increasing ion concentrations and extracellular space tortuosity (33, 34). Other things equal these changes might increase susceptibility to SD (34), though the reality might be complex; e.g. increased tortuosity might contribute to local increases in $[K^+]_e$, but might hinder propagation. Our data do not allow us to measure all of the relevant parameters, but they strongly suggest that even in the presence of factors that might increase SD susceptibility, the reduction in neuronal intrinsic excitability predominates 48 h after CCI injury.

Our data might appear to contradict work in brain slices, showing that neuronal volume perturbations with hypo-osmotic agents are associated with increases in excitability, and that a hyperosmotic agent, mannitol, is linked with decreases in seizure-like activity. There may be key

differences in preparation that account for this discrepancy. Brain slice preparations typically use osmotic changes to study seizure-like activity (35–40). Acute hypo-osmolality in vitro can enhance $[K^+]_e$ concentration, field effects, and EPSP input by reducing extracellular space through astrocytic swelling, ultimately enhancing neuronal synchronization and seizure activity (35–40). However, acute osmotic changes (minutes) have little effect on neuronal volume (41–43), likely because neurons lack aquaporin channels (41–43) (but see (44)), and neurons swell on longer time scales (hours-days) with regulated mechanisms (42). Moreover, changing extracellular osmolality does not change the intrinsic membrane properties of neurons (38, 39, 45, 46). To our knowledge, no studies have explored the effects of osmolality on endogenous membrane properties in vivo. Acute osmotically mediated changes in excitability observed in brain slices likely model a mechanistically relevant component of brain injury, as alterations in EPSC input (possibly mediated by increases in extracellular glutamate) and ionic changes (increases in $[K^+]_e$) can occur early in injury. From the translational standpoint, the net effect of the multiple changes associated with injury may be more important. Our data shows that as neurons swell after TBI, both neuronal membrane excitability and network activity decrease. This is further supported by other in vivo work which shows reduced sensory-evoked neuronal firing after TBI (47, 48). In sum, though our data may appear contradictory to acute osmotically evoked seizure models in brain slices, this in vivo work is probably the most predictive translationally.

***No difference in lesion size or cell death after bumetanide treatment***

We tested whether the inhibition of NKCC1 with bumetanide which is responsible for increased excitability was also responsible for the changes in cortical lesion size and neurodegeneration. Data shows that the area of cortical contusion lesion in the ipsilateral cortex as

a percentage of the contralateral uninjured cortex was 15% in CCI-vehicle group, whereas the area of lesion was 14.26% in the CCI-bumetanide group at 48 h post-injury. No changes in lesion area were detected between vehicle and bumetanide-treated groups ($p > 0.05$, two-sided unpaired t-test; n = 5 mice per group; **Data not shown**). Analysis of flurojade (FJB) staining indicated that there was substantial cell degeneration at 48 h after CCI injury. Robust staining was observed on the ipsilateral side to the impact in the perilesional area (i.e., around the lesion site). As expected, we did not see any cell death in sham-treated animals. In order to compare FJB staining between vehicle and bumetanide groups, we measured number of positive neurons in the perilesional area. There was no difference between groups ($p > 0.05$, two-sided unpaired t-test; n = 5 mice per group; **Data not shown**). Importantly, the blockade of neuronal swelling with bumetanide increases the incidence of SD and seizures. Though we observed no expansion of lesion size and neuronal death, it is difficult to conclude that these might not be damaging events, given evidence for both SD and seizures in worsening outcomes in brain injury (49, 50).

***Spatial profile of CCI-associated changes in excitability***

Our seizure data affirms that excitability effects observed after CCI are not exclusively associated with pericontusional domains but rather have global effects on network activity. We show increases in seizure susceptibility after edema treatment by using the minimal clonic seizure model with corneal stimulation (51). This protocol induces seizure phenotypes illustrating consistent pattern of whole brain activation: corneal stimulation likely takes advantage of visual pathways and is known to involve forebrain (52, 53). Moreover, seizure behavior such as forelimb clonus was not lateralized (i.e., restricted to one forepaw). Prior work supports that TBI is associated with both ipsi- and contralateral changes in KCC2 expression, suggesting that we might

anticipate a similar effect in the non-injured hemisphere (54). These observations do not prove that there has been a change in baseline excitability beyond the 'injury penumbra;' however it does show that the excitability changes we observe, whether they be local or more diffuse, have widespread effects on network excitability.

## Supplemental Figures

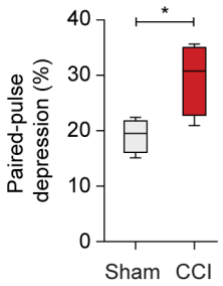


**Supplemental Figure 1.** *Paired pulse depression to sensory stimulation after CCI.* There was depression of the second stimulus-evoked response, relative to the first response, in neurons of both sham and CCI mice. This depression is more dramatic in neurons of CCI mice (**p* = 0.02; one-sided Mann-Whitney test; n = 4 neurons, 4 mice per group).

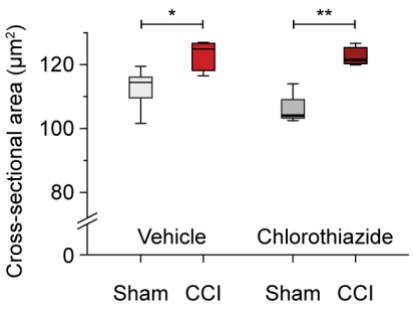


**Supplemental Figure 2.** *Chlorothiazide* (10 mg/kg, i.p.)*, a peripherally active diuretic, lacks effects on neuronal edema.* We imaged neuronal cross-sectional area with in vivo two-photon microscopy of GCaMP6f-injected mice 48 h post-CCI/sham treated with chlorothiazide. Similar to CCI vehicle-treated neurons with increased cross-sectional area relative to sham-vehicle group, CCI neurons treated with CTZ also have larger cross-sectional area, relative to sham-CTZ neurons ($p$ = 0.001, one-way ANOVA with Bonferroni's multiple comparisons test; CCI-CTZ vs sham-CTZ: **$p$ < 0.01, CCI-vehicle vs sham-vehicle: *$p$ < 0.05; n = 49-66 cells, 3-5 mice per group).

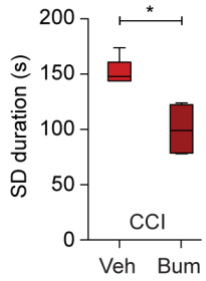


**Supplemental Figure 3.** *Bumetanide reduces duration of CCI-evoked spontaneous spreading depolarization activity.* In CCI-vehicle treated animals, SD activity was sustained for approximately 150 s. However, the duration of SD in CCI animals was significantly reduced following bumetanide treatment, compared to CCI-vehicle (*$p$ = 0.01, two-sided Mann-Whitney test; n = 4-5 mice per group).

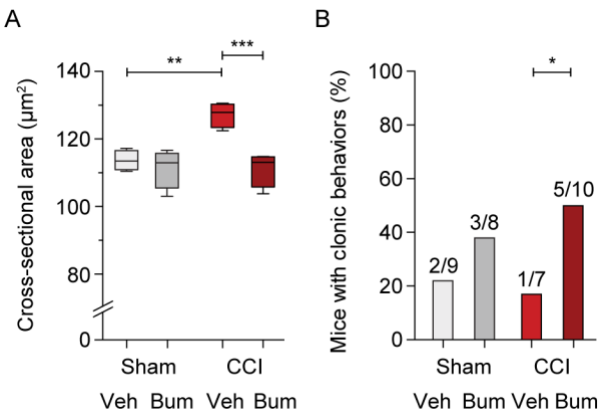


**Supplemental Figure 4.** *Bumetanide administered immediately post-CCI eliminates neuronal edema and increases network excitability.* **A.** Quantification of neuronal cross-sectional area shows reversal of edema with bumetanide post-CCI treatment ($p = 0.001$, one-way ANOVA with Bonferroni multiple comparisons test; CCI-bumetanide vs vehicle: $^{**}p < 0.01$, CCI-vehicle vs sham-vehicle: $^{**}p < 0.01$; n = 32-70 neurons, 4-5 mice per group). **B.** Bumetanide induced reduction of post-CCI neuronal edema increases network excitability, as assessed by increases in the percentage of animals exhibiting seizures (CCI- bumetanide vs vehicle: $^{*}p = 0.04$, ChiSqu test; n = 8-12 mice per group; number of mice showing seizures and group size are indicated for each group.).

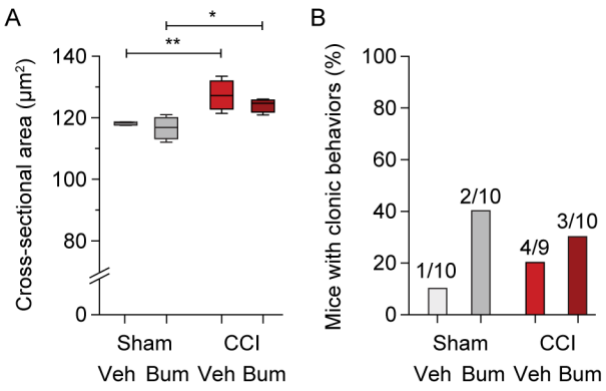


**Supplemental Figure 5.** *Bumetanide administered at 48 h post-CCI fails to reduce neuronal swelling.* **A.** Quantification of neuronal cross-sectional area shows no changes in neuronal edema with bumetanide ($p = 0.001$, one-way ANOVA with Bonferroni multiple comparisons test; CCI-bumetanide vs sham-bumetanide: $*p < 0.05$, CCI-vehicle vs sham-vehicle: $**p < 0.01$; n = 42-55 neurons, 4 mice per group). **B.** Plot showing the percentage of animals with seizure activity (%) in sham and CCI animals treated with vehicle or bumetanide. Consistent with no effect on neuronal swelling, bumetanide injected at 48 h post-CCI does not affect seizure susceptibility (CCI-bumetanide vs vehicle: $p > 0.05$, ChiSqu test; n = 10 mice per group; number of mice showing seizures and group size are indicated for each group.).

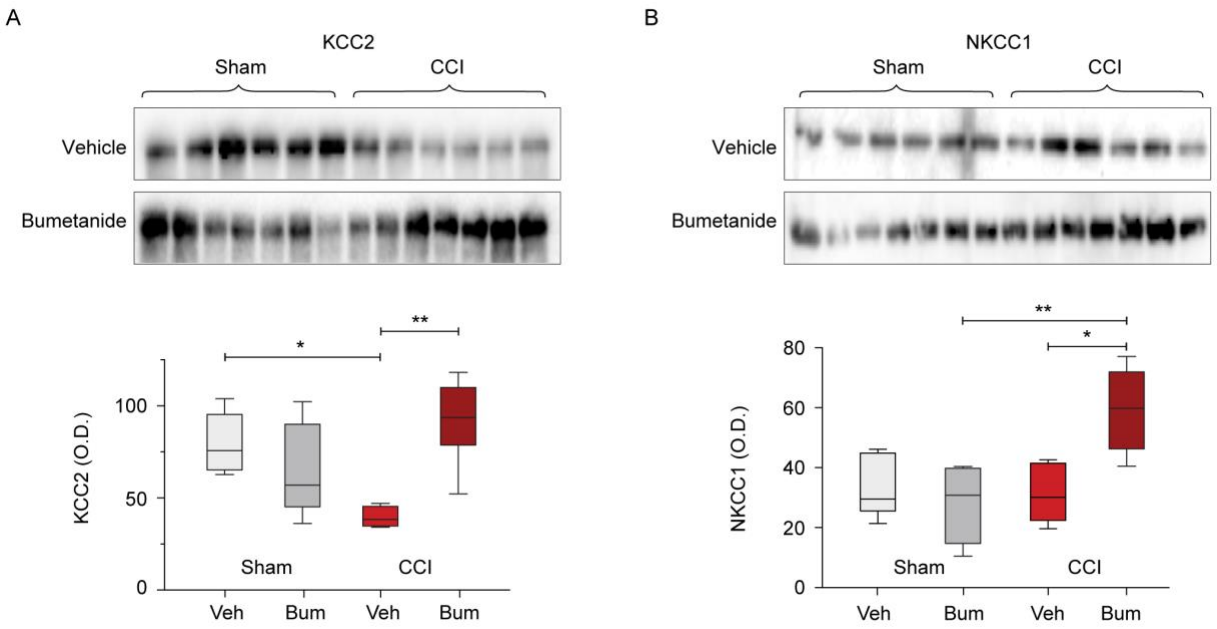


**Supplemental Figure 6.** *Cation chloride cotransporter expression in the injured cortex 2 h after CCI*. **A.** The protein expression level of KCC2 was significantly decreased 2 h after TBI. Bumetanide significantly elevated KCC2 expression in CCI mice, relative to CCI-vehicle animals ($p = 0.005$, Kruskal-Wallis test with Dunn's multiple comparisons; CCI-bumetanide vs vehicle: $^{**}p < 0.01$; CCI-bumetanide vs sham-bumetanide: $p > 0.05$, CCI-vehicle vs sham-vehicle: $^{*}p < 0.05$; n = 5-6 mice per group). **B.** Although, NKCC1 expression levels were unaltered after TBI, pre-treatment with bumetanide significantly upregulated NKCC1 expression at 2 h after TBI, relative to CCI-vehicle and sham-bumetanide ($p = 0.008$, Kruskal-Wallis test with Dunn's multiple comparisons; CCI-bumetanide vs vehicle: $^{*}p < 0.05$; CCI-bumetanide vs sham-bumetanide: $^{**}p < 0.01$, CCI-vehicle vs sham-vehicle: $p > 0.05$; n = 5-6 mice per group). All lanes within the boxes were run on the same gels.

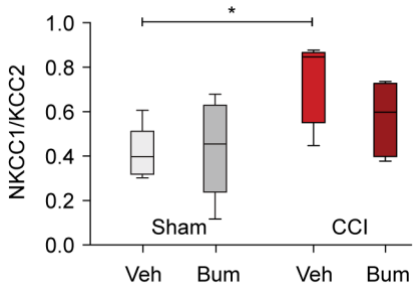


**Supplemental Figure 7.** *Alterations in the expression ratio of chloride cotransporters 2 h after traumatic brain injury.* Increase in the ratio of NKCC1 to KCC2 expression levels in CCI-vehicle group, compared to sham-vehicle. This increase was moderately reversed by bumetanide when given 30 min prior to CCI injury ($p = 0.03$, Kruskal-Wallis test with Dunn's multiple comparisons; CCI-bumetanide vs vehicle: $p > 0.05$, CCI-vehicle vs sham-vehicle: $*p < 0.05$; n = 5-7 mice per group).

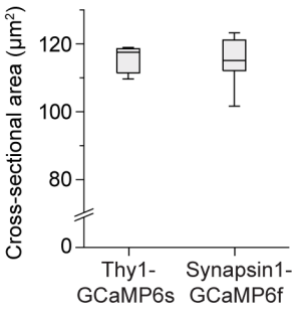


**Supplemental Figure 8.** *Cell size measurements of layer 2/3 sensory cortical neurons in Thy1-GCaMP6s mice and Synapsin1-driven-GCaMP6f-injected mice.* Somatic area was comparable between two groups ($p > 0.05$, two-sided unpaired t-test; n = 9-12 mice per group). Due to no differences in cell size based on the two methods, we combined these data into one experimental group (i.e., '*bumetanide administered immediately post-CCI*').

**Availability of Data:**

All raw data generated in this study, including electrophysiology, two photon imaging, histology, and Western blot, as well as all analysis and statistical data, are available upon request from the corresponding authors: Punam A. Sawant-Pokam and K.C. Brennan, 383 Colorow Drive Room 280A, Department of Neurology, Salt Lake City, Utah 84108, USA. Phone: 801.512.4282 (PASP), 801.581.8129 (KCB); Email: punam.pokam@utah.edu, k.c.brennan@hsc.utah.edu.

## References


1. Kitamura K, Judkewitz B, Kano M, Denk W, Häusser M. Targeted patch-clamp recordings and single-cell electroporation of unlabeled neurons in vivo. *Nature Methods.* 2007;5:61.

2. Brennan KC, Romero-Reyes M, López Valdés HE, Arnold AP, Charles AC. Reduced threshold for cortical spreading depression in female mice. *Annals of Neurology.* 2007;61(6):603–606.

3. Bogdanov VB et al. Susceptibility of Primary Sensory Cortex to Spreading Depolarizations. *J. Neurosci.* 2016;36(17):4733.

4. Schneider CA, Rasband WS, Eliceiri KW. NIH Image to ImageJ: 25 years of image analysis. *Nature methods*. 2012;9(7):671–675.

5. Scholl EA, Dudek FE, Ekstrand JJ. Neuronal degeneration is observed in multiple regions outside the hippocampus after lithium pilocarpine-induced status epilepticus in the immature rat. *Neuroscience.* 2013;252:45–59.

6. Sivakumaran S, Maguire J. Bumetanide reduces seizure progression and the development of pharmacoresistant status epilepticus. *Epilepsia.* 2016;57(2):222–232.

7. Sawant-Pokam P, Suryavanshi P, Dudek F, Brennan K. Mechanisms of Neuronal Silencing After Cortical Spreading Depression. *Cerebral Cortex.* 2017;27:1311–1325.

8. Dana H et al. Thy1-GCaMP6 transgenic mice for neuronal population imaging in vivo. *PloS one.* 2014;9(9):e108697–e108697.

9. Han EB, Stevens CF. Development regulates a switch between post- and presynaptic strengthening in response to activity deprivation. *Proceedings of the National Academy of Sciences of the United States of America.* 2009;106(26):10817–10822.

10. Fatt P, Katz B. Spontaneous subthreshold activity at motor nerve endings. *The Journal of physiology.* 1952;117(1):109–128.

11. Carron SF, Alwis DS, Rajan R. Traumatic Brain Injury and Neuronal Functionality Changes in Sensory Cortex. *Front Syst Neurosci.* 2016;10:47.

12. Sanchez-Vives MV et al. Inhibitory Modulation of Cortical Up States. *Journal of Neurophysiology.* 2010;104(3):1314–1324.

13. Wang M, Ramos B, McCormick D. α2A-Adrenoceptors Strengthen Working Memory Networks by Inhibiting cAMP-HCN Channel Signaling in Prefrontal Cortex. *Cell.* 2007;129(2):397–410.

14. Magee J, Hoffman D, Colbert C, Johnston D. Electrical and calcium signaling in dendrites of hippocampal pyramidal neurons. *Annu. Rev. Physiol.* 1998;60(1):327–346.

15. Poolos NP, Migliore M, Johnston D. Pharmacological upregulation of h-channels reduces the excitability of pyramidal neuron dendrites. *Nature Neuroscience.* 2002;5:767.

16. Deng P, Xu ZC. Contribution of Ih to Neuronal Damage in the Hippocampus after Traumatic Brain Injury in Rats. *Journal of Neurotrauma.* 2011;28(7):1173–1183.

17. Larkum ME, Waters J, Sakmann B, Helmchen F. Dendritic Spikes in Apical Dendrites of Neocortical Layer 2/3 Pyramidal Neurons. *J. Neurosci.* 2007;27(34):8999.

18. Sheets PL et al. Corticospinal-specific HCN expression in mouse motor cortex: I(h)-dependent synaptic integration as a candidate microcircuit mechanism involved in motor control. *Journal of Neurophysiology.* 2011;106(5):2216–2231.

19. Thuault SJ et al. Prefrontal Cortex HCN1 Channels Enable Intrinsic Persistent Neural Firing and Executive Memory Function. *J. Neurosci.* 2013;33(34):13583.

20. von Baumgarten L, Trabold R, Thal S, Back T, Plesnila N. Role of Cortical Spreading Depressions for Secondary Brain Damage after Traumatic Brain Injury in Mice. *J Cereb Blood Flow Metab.* 2008;28(7):1353–1360.

21. Rogatsky GG, Sonn J, Kamenir Y, Zarchin N, Mayevsky A. Relationship between Intracranial Pressure and Cortical Spreading Depression following Fluid Percussion Brain Injury in Rats. *Journal of Neurotrauma.* 2003;20(12):1315–1325.

22. Zhou, Gordon, Feighan, MacVicar. Transient swelling, acidification, and mitochondrial depolarization occurs in neurons but not astrocytes during spreading depression. *Cerebral Cortex.* 2010;20(11):2614–2624.

23. Takano, Tian, Peng, Lou, Nedergaard. Cortical spreading depression causes and coincides with tissue hypoxia. *Nature neuroscience.* 2007;10:754–762.

24. Mestre H et al. Cerebrospinal fluid influx drives acute ischemic tissue swelling. *Science.* 2020;367(6483):eaax7171.

25. Pacheco JM et al. Spreading Depolarizations Occur in Mild Traumatic Brain Injuries and Are Associated with Postinjury Behavior. *eNeuro.* 2019;6(6):ENEURO.0070-19.2019

26. Tang YT et al. Minimum conditions for the induction of cortical spreading depression in brain slices. *J Neurophysiol.* 2014;112(10):2572–2579.

27. Liu H-T, Tashmukhamedov BA, Inoue H, Okada Y, Sabirov RZ. Roles of two types of anion channels in glutamate release from mouse astrocytes under ischemic or osmotic stress. *Glia.* 2006;54(5):343–357.

28. Kimelberg HK, Rutledge E, Goderie S, Charniga C. Astrocytic Swelling Due to Hypotonic or High K+ Medium Causes Inhibition of Glutamate and Aspartate Uptake and Increases Their Release. *J Cereb Blood Flow Metab.* 1995;15(3):409–416.

29. Abdullaev IF, Rudkouskaya A, Schools GP, Kimelberg HK, Mongin AA. Pharmacological comparison of swelling-activated excitatory amino acid release and Cl- currents in cultured rat astrocytes. *The Journal of physiology.* 2006;572(Pt 3):677–689.

30. Lauderdale K et al. Osmotic Edema Rapidly Increases Neuronal Excitability Through Activation of NMDA Receptor-Dependent Slow Inward Currents in Juvenile and Adult Hippocampus. *ASN neuro.* 2015;7(5):1759091415605115.

31. Jayakumar AR et al. Na-K-Cl Cotransporter-1 in the mechanism of ammonia-induced astrocyte swelling. *The Journal of biological chemistry.* 2008;283(49):33874–33882.

32. Töpfer M et al. Consequences of inhibition of bumetanide metabolism in rodents on brain penetration and effects of bumetanide in chronic models of epilepsy. *European Journal of Neuroscience.* 2014;39(4):673–687.

33. Ullah G, Wei Y, Dahlem MA, Wechselberger M, Schiff SJ. The Role of Cell Volume in the Dynamics of Seizure, Spreading Depression, and Anoxic Depolarization. *PLoS computational biology.* 2015;11(8):e1004414.

34. Spong KE, Chin B, Witiuk KLM, Robertson RM. Cell swelling increases the severity of spreading depression in Locusta migratoria. *Journal of Neurophysiology.* 2015;114(6):3111–3120.

35. Dudek FE, Obenaus A, Tasker JG. Osmolality-induced changes in extracellular volume alter epileptiform bursts independent of chemical synapses in the rat: Importance of non-synaptic mechanisms in hippocampal epileptogenesis. *Neuroscience Letters.* 1990;120(2):267–270.

36. Haglund MM, Hochman DW. Furosemide and Mannitol Suppression of Epileptic Activity in the Human Brain. *Journal of Neurophysiology.* 2005;94(2):907–918.

37. Jefferys JG. Nonsynaptic modulation of neuronal activity in the brain: electric currents and extracellular ions. *Physiological Reviews.* 1995;75(4):689–723.

38. Rosen AS, Andrew RD. Osmotic effects upon excitability in rat neocortical slices. *Neuroscience.* 1990;38(3):579–590.

39. Andrew RD, Fagan M, Ballyk BA, Rosen AS. Seizure susceptibility and the osmotic state. *Brain Research.* 1989;498(1):175–180.

40. Dudek FE, Yasumura T, Rash JE. Non-Synaptic mechanisms in seizures and epileptogenesis. *Cell Biology International.* 1998;22(11-12):793–805.

509 41. Andrew RD, Labron MW, Boehnke SE, Carnduff L, Kirov SA. Physiological Evidence That
510 Pyramidal Neurons Lack Functional Water Channels. *Cerebral Cortex.* 2006;17(4):787–802.

511 42. Glykys et al. Chloride Dysregulation, Seizures, and Cerebral Edema: A Relationship with
512 Therapeutic Potential. *Trends in Neurosciences.* 2017;40:276–294.

513 43. Caspi A, Benninger F, Yaari Y. KV7/M Channels Mediate Osmotic Modulation of Intrinsic
514 Neuronal Excitability. *J. Neurosci.* 2009;29(36):11098.

515 44. Murphy TR et al. Hippocampal and Cortical Pyramidal Neurons Swell in Parallel with
516 Astrocytes during Acute Hypoosmolar Stress. *Frontiers in Cellular Neuroscience.* 2017;11:275.

517 45. Azouz R, Alroy G, Yaari Y. Modulation of endogenous firing patterns by osmolarity in rat
518 hippocampal neurones. *J Physiol.* 1997;502:175–187.

519 46. Rosen AS, David Andrew R. Glucose concentration inversely alters neocortical slice
520 excitability through an osmotic effect. *Brain Research.* 1991;555(1):58–64.

521 47. Johnstone VPA, Shultz SR, Yan EB, O'Brien TJ, Rajan R. The Acute Phase of Mild
522 Traumatic Brain Injury Is Characterized by a Distance-Dependent Neuronal Hypoactivity.
523 *Journal of Neurotrauma.* 2014;31(22):1881–1895.

524 48. Johnstone VPA, Yan EB, Alwis DS, Rajan R. Cortical Hypoexcitation Defines Neuronal
525 Responses in the Immediate Aftermath of Traumatic Brain Injury. *PLOS ONE.*
526 2013;8(5):e63454.

527 49. Fabricius M et al. Cortical spreading depression and peri-infarct depolarization in acutely
528 injured human cerebral cortex. *Brain.* 2006;129(3):778–790.

529 50. Hartings JA et al. Spreading depolarizations have prolonged direct current shifts and are
530 associated with poor outcome in brain trauma. *Brain.* 2011;134(5):1529–1540.

531 51. Otto JF et al. Electroconvulsive seizure thresholds and kindling acquisition rates are altered
532 in mouse models of human KCNQ2 and KCNQ3 mutations for benign familial neonatal
533 convulsions. *Epilepsia.* 2009;50(7):1752–1759.

534 52. Browning RA, Nelson DK. Modification of electroshock and pentylenetetrazol seizure
535 patterns in rats affer precollicular transections. *Experimental Neurology.* 1986;93(3):546–556.

536 53. Eells JB, Clough RW, Browning RA, Jobe PC. Comparative fos immunoreactivity in the
537 brain after forebrain, brainstem, or combined seizures induced by electroshock,
538 pentylenetetrazol, focally induced and audiogenic seizures in rats. *Neuroscience.*
539 2004;123(1):279–292.

540 54. Goubert E et al. Bumetanide Prevents Brain Trauma-Induced Depressive-Like Behavior.
541 *Frontiers in Molecular Neuroscience.* 2019;12:12.